J. Fluid Mech. (1982), *vol.* 124, *pp.* 363–390
Printed in Great Britain

The use of multiple wall probes to identify coherent flow patterns in the viscous wall region

By J. H. A. HOGENES† AND THOMAS J. HANRATTY
Department of Chemical Engineering, University of Illinois, Urbana

(Received 6 August 1980 and in revised form 20 April 1982)

Multiprobe techniques were used to study the coherent flow-oriented eddy pattern that exists close to a wall in a turbulent flow. Simultaneous measurements of the spanwise component s_z of the fluctuating wall velocity gradient at a number of locations in the spanwise direction were used to detect different aspects of the secondary flows that are superimposed on the mean flow. Conditionally averaged measurements of the streamwise component of the wall velocity gradient and of the streamwise component of the velocity at a number of locations on a line perpendicular to the wall show how the streamwise velocity fluctuations are related to the eddy structure, as detected by the $s_z(z)$ variation.

The results are consistent with the suggestion by Sirkar & Hanratty (1970*a*) that the flow-oriented eddies are approximately homogeneous in the flow direction and, on average, have inflows and outflows of equal magnitude coupled in the spanwise direction; i.e. they may be modelled, on average, by a sinusoidal $s_z(z)$ variation with dimensionless wavelength $\lambda^+ = 100$. The results are also consistent with explanations by Fortuna and Hanratty (see Fortuna 1971; Hanratty, Chorn & Hatziavramidis 1977) and by Hatziavramidis & Hanratty (1979) of how these secondary flows are affecting momentum transport to the wall.

1. Introduction

A number of studies in recent years have indicated that turbulent flow close to a solid boundary is dominated by coherent structures that are greatly elongated in the streamwise direction. This paper shows how multipoint measurements of the velocity gradient at the wall can be used to detect the occurrence of these structures. It applies conditional sampling techniques to identify how these secondary flows evolve in time, how they cause changes in the axial component of momentum, and how they are responsible for the emergence of low-momentum fluid from the wall. In a later paper (Nikolaides, Lau & Hanratty 1982) these multipoint identification techniques are used to examine the origin of flow-oriented wall eddies. The work described in both papers are attempts to explore the extent to which the simplified eddy models developed by Sirkar & Hanratty (1970*a*), Fortuna and Hanratty (see Hanratty, Chorn & Hatziavramidis 1977; Fortuna 1971), and Hatziavramidis & Hanratty (1979) describe the kinematics of the flow in the viscous wall region.

Extensive measurements of the two-point spatial correlation of the different velocity components, made by Grant (1958) just outside the viscous wall region ($y^+ \approx 35$), supply indirect evidence for flow-oriented structures in the region $y^+ < 35$. On the basis of these measurements, Townsend (1958) postulated that the eddy

† Present address: Gasunie, Groningen, The Netherlands.

structure in the constant-stress layer is dominated by two-dimensional jets, originating at the edge of the 'viscous layer', with a surrounding induced flow represented as two counter-rotating masses of fluid. Townsend pictured these jets as being of comparatively long and indeterminate length in the direction of mean flow.

The first direct evidence for flow-oriented eddies in the viscous wall region was obtained from studies of patterns formed from injected dye and from measurements of the fluctuating velocity gradient at the wall.

Beatty, Ferrell and Richardson (see Corrsin 1956) pumped a dye solution through a pipe and observed the residual dye forming streamwise filaments at the wall after flushing with water. Hama (see Corrsin 1956) and Kline & Runstadler (1959) observed the formation of a streaky structure downstream from a wall slot through which dye was injected. Kline & Runstadler found that the regions in the wall streaks (called by them 'islands of hesitation') have low velocities in the streamwise direction. In futher studies of dye filaments, as well as of lines of hydrogen bubbles, Kline *et al.* (1967) identified the 'bursting' phenomenon as a violent interaction of low-speed fluid, lifted from the wall, with high-speed fluid outside the viscous wall region. Kim, Kline & Reynolds (1971) found that these 'bursts' are associated with large Reynolds stresses, and therefore with a large production of turbulence. This suggested that the flow-oriented coherent structures close to the wall could be of primary importance in understanding how wall turbulence is sustained and has led to considerable effort to obtain a more detailed description of these structures and how they interact with the outer flow.

Reiss & Hanratty (1962, 1963) used electrochemical techniques to determine the spatial correlation of the fluctuating velocity gradient **s** at the wall. They found that the scale of the streamwise component s_x is at least an order of magnitude smaller in the spanwise direction than in the flow direction, thus suggesting that the elongated eddy structures detected by Grant just outside the viscous wall layer extend right down to the wall. Willmarth & Tu (1967) confirmed the above results by carrying out measurements with a number of hot wires glued onto the wall at $y^+ = 5$. Bakewell & Lumley (1967) made extensive measurements of the streamwise component of the velocity throughout the viscous wall region in a specially designed glycerol tunnel. By using mixing-length-type arguments and the assumption of homogeneity in the direction of flow, they suggested that eddy structures of the type proposed by Townsend extend right to the wall.

By using a pair of electrodes in a chevron arrangement flush with the wall, Sirkar & Hanratty (1970*b*) were able to measure the spanwise component s_z of the velocity gradient at the wall as well as the streamwise component. They showed that there are large spanwise movements of fluid right at the wall, s_z being about one-third of s_x. This result, as well as the previous observations of elongated eddy structures, prompted Sirkar & Hanratty (1970*a*) to suggest that flow in the vicinity of the wall may be considered as dominated by a secondary flow, homogeneous in the streamwise direction, of the type shown in figure 1 (*a*). This is essentially the same as the eddy model suggested by Bakewell & Lumley except that the inflows at the wall are assumed to be of the same magnitude as the outflows.

Fortuna and Hanratty (see Hanratty *et al.* 1977; Fortuna 1971) used this model and a pseudosteady-state assumption to calculate the time-averaged velocity profile and the fluctuations in the streamwise velocity component. The eddies shown in figure 1 (*a*) were pictured as bringing high-momentum fluid from the outer flow towards the wall at location A, to exchange momentum with the wall as they transport fluid

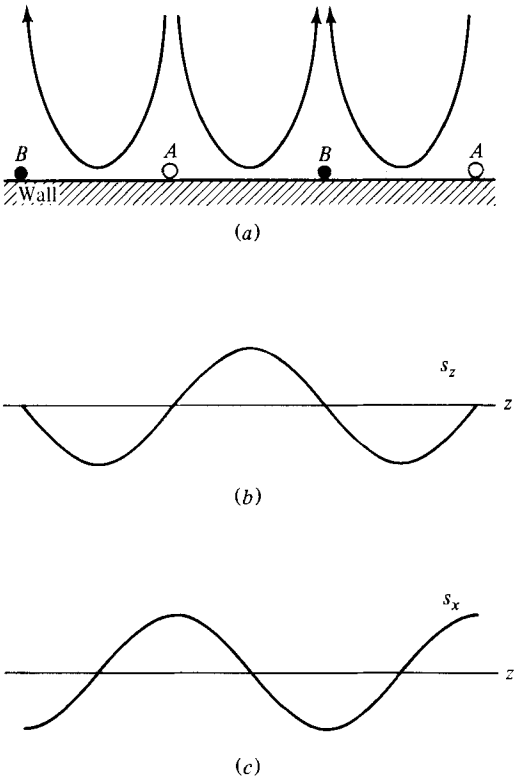

FIGURE 1. Idealized coherent eddy structure.

from A to B, and to carry low-momentum fluid away from the wall at location B. A consequence of this exchange between the secondary flow and the wall and of the convection of negative momentum by the secondary flow is that the streamwise component s_x of the fluctuating velocity gradient at the wall should have a definite phase relation to the spanwise component s_z, as shown in figures 1(*b*,*c*). The calculations by Fortuna showed that the eddy motions produce large fluctuations in the streamwise component of the velocity that could be responsible for the observed maximum in the turbulence intensity at $y^+ \approx 15$. Good agreement was also obtained between calculations and the measured variation of the time-averaged streamwise component of the velocity with distance from the wall. Results of a similar type have also been obtained recently by Coles (1978), who was exploring whether a model based on a Taylor–Görtler instability can describe 'longitudinal sublayer vortices'.

It was implied in the work by Fortuna that the secondary flows detected by the electrochemical wall probes are associated with spanwise velocity fluctuations at $y^+ \approx 30$–40 and that they are not necessarily directly associated with vortical motions within the viscous wall region. Hatziavramidis & Hanratty (1979) explored this notion by solving the equations of motion numerically for a flow driven by a spanwise velocity at $y^+ \approx 30$–40 that is periodic in the spanwise direction and in time. By using a wavelength and period approximately equal to the observed spacing of flow-oriented structures and the time interval between bursts, good agreement was obtained between the calculated velocity field and many aspects of the fluctuating flow in the viscous wall region that have been observed. Such a model predicts the periodic emergence of low-momentum fluid from the wall, but does not predict the intricate flow patterns that result from the interaction of this low-momentum fluid with the

outer flow. Because the flow does not change immediately with changes in the outer velocity there is a lag between the velocities at the wall and the outer flow. Hatziavramidis calculates a maximum in the correlation between the axial velocity at $y^+ = 33$ and at the wall if the outer velocities are delayed by $\Delta T^+ = 14$. This compares reasonably well with the value of $\Delta T^+ = 20$ measured by Kreplin & Eckelmann (1979). Transient vortical flow structures in the (y, z)-plane also emerge from the calculation by Hatziavramidis because the spanwise velocity component close to the wall does not change direction immediately with a change in the direction of the spanwise velocity component at $y^+ \approx 30$–40.

Experimental support for the idealized model of the wall eddies developed by Sirkar and Fortuna has been presented by Lee, Eckelmann & Hanratty (1974), who used an array of chevron electrode pairs to measure both components of the fluctuating velocity gradient simultaneously at a number of locations on the wall. The instantaneous spanwise variation in s_z was found to have, on average, the type pattern shown in figure 1 (*b*) in that the observed inflows and outflows close to the wall are of the same magnitude. Measurements of the spanwise distance between zero crossings gave a distribution of lengths whose average is equal to the spacing of the streaky structures observed by Kline and his coworkers. Measurements of the correlations between s_x at a given spanwise location z and of s_z at location $z + \Delta z$ reveal a maximum at $\Delta z \approx \frac{1}{4}\lambda$ as would be suggested from the patterns shown in figures 1 (*b*, *c*).

Techniques similar to those developed by Sirkar and by Lee *et al.* were employed in experiments recently conducted at Göttingen (Blackwelder & Eckelmann 1978, 1979; Kreplin & Eckelmann 1979). These experiments also support a model for the flow close to the wall of the type shown in figure 1 (see figure 2 of Blackwelder & Eckelmann 1979). However, on the basis of correlation measurements between s_z and the spacewise component of the velocity fluctuations at different distances from the wall, Blackwelder & Eckelmann argue that the secondary flows at the wall are part of a vortex structure whose middle lies approximately at $y^+ = 20$–30. Kreplin & Eckelmann develop this notion further by suggesting that the vortices are inclined in the flow direction and that their angle of inclination continues to decrease until they are destroyed. They estimate that the average minimum distance of the vortex centre from the wall is $y^+ \approx 30$.

Measurements of s_z and s_x patterns at the wall are therefore in good agreement with the idealized eddy model given in figure 1. The support for the notion that changes in the s_z patterns reflect changes in the velocity field throughout the viscous wall region is weaker. Furthermore, the value of a simple model such as this in accounting for the momentum transport to the wall and for the transfer of energy from the mean flow to the turbulence needs to be established. Some encouragement along these lines can be obtained from the correlation measurements obtained at Göttingen and from the calculations carried out by Fortuna and Hatziavramidis. However, stronger support can be obtained from conditionally averaged velocity measurements, which reflect in a direct way the relation of the velocity field to changes in the eddy structure and which give information on how the eddy structure and velocity field evolve in time.

The approach taken by us in carrying out such conditional averaging is to compare measurements of s_z at a number of z-locations with the pattern shown in figure 1 (*b*) to determine whether a strong eddy exists. Probes that are mass-transfer analogues of the hot-film anemometer are located over the centre of this array, defined as $z = 0$, in order to measure properties of the velocity field. Four aspects of strong wall eddies are defined. Negative or positive values of ds_z/dz at $z = 0$ indicate

repectively that a strong inflow or a strong outflow would be sampled by the fluid probes. Maxima or minima in $s_z(z)$ at a fixed time indicate strong positive or negative spanwise flows and, on average, a coupled inflow and outflow at distances of $\Delta z^+ \approx 25$ from the centre of the wall probe array.

In this paper the influence of these eddies, defined in terms of the $s_z(z)$ pattern, on the axial velocity component is examined by studying how the $s_x(z)$ pattern and the streamwise velocity profile at $z = 0$ are associated with changes in the eddy pattern. The results of these studies do not provide any information on whether the wall eddies should be pictured as vortical structures or as flows that are merely associated with spanwise velocity fluctuations at $y^+ = 30$–40. This type of question is addressed in another paper (Nikolaides *et al.* 1982), in which we study the relation of the spanwise velocity at different values of x, y and z to changes in the eddy structure as detected by multiple wall probes.

The work to be presented here is of interest on three counts: (i) it describes a new method, involving multiple wall probes, of obtaining conditionally averaged measurements of flow-oriented wall eddies; (ii) it indicates how the wall eddies and the associated streamwise velocity field evolve in time; (iii) it provides further support for using the idealized eddy model to describe momentum transport between the wall and the fluid and to account for the origin of the low-momentum fluid that has been observed to emerge intermittently from the wall region.

Blackwelder & Eckelmann (1979) have used two pairs of chevron electrodes at a spacing of $\Delta z^+ = 20$ to detect outflows from the wall at $z^+ \approx 0$ in a few experiments in which they tried to detect whether an 'upstream structure or instability mechanism' is related to or causes the flow-oriented wall eddies. Aside from this work, all of the previous applications of conditional sampling techniques to study the viscous wall region have involved single-probe detection devices. The chief emphasis of these researches has been to develop an instrumental method for detecting bursting. Offen & Kline (1974) have compared various burst-detection schemes and concluded that none of them 'correlated very well with the visual indications of bursting or with any other scheme' and that 'there remain serious questions about what events are measured by each technique'. Willmarth (1975) also points out that the burst-detection schemes suggested by Blackwelder & Kaplan (1976) and by Willmarth & Lu (1971) give quite different time variations of the uv-signal. Results of this type show the difficulty of extracting from measurements of the time variation of the velocity signal at a given location in the flow field information about the spatial variation of the velocity; i.e. the structure.

The experiments discussed in this paper used the fully developed flow of an electrolyte in a pipe with an internal diameter of 19·37 cm. Ten chevron pairs of electrodes equally spaced in the spanwise direction were used to measure the axial and spanwise components of the fluctuating velocity gradient at the wall. An eight-sensor fluid probe (i.e. a rake) with fixed distances between its sensors was placed downstream from the wall probes. The rake was used to measure the average and the fluctuating axial velocity components at seven positions in the fluid and the radial velocity component at one position. The measurements were obtained at a Reynolds number of 29600.

During an experiment the 28 analog signals from the fluid and wall probes were digitalized with a sample frequency of 30 Hz for approximately 5·5 minutes until 10000 data points were obtained from each of the signals. These data were transferred to a Cyber-175 digital computer for analysis. Events defining zero time for conditional averaging were obtained from the time variation of s_z at multiple locations in the

x^+ \ Rake position	Probe	1	2	3	4	5	6	7
30		14	22	30	39	56	75	106
60		11	19	27	36	53	72	103
90		8	16	24	33	50	69	100

TABLE 1. Dimensionless distance y^+ of the fluid probes (1, 2, ..., 7) from the wall

$Re = 29600$	$\langle s_x^2 \rangle^{\frac{1}{2}} = 22{\cdot}8\ \text{s}^{-1}$	$F_S = 30\ \text{s}^{-1}$
$D_t = 19{\cdot}37$ cm	$\langle s_z^2 \rangle^{\frac{1}{2}} = 7{\cdot}43\ \text{s}^{-1}$	$N_D = 10000$
$U_b = 13{\cdot}55\ \text{cm s}^{-1}$	$\nu = 0{\cdot}00886\ \text{cm}^2\ \text{s}^{-1}$	$T_D^+ = 20000$
$\langle S \rangle = 63{\cdot}4\ \text{s}^{-1}$	$C_b = 6{\cdot}28 \times 10^{-6}\ \text{mol cm}^{-3}$	$E_D \approx 100$

TABLE 2

spanwise direction. The average behaviour of the x-component of the velocity field during these events was determined from the measurements of the streamwise components s_x of the fluctuating velocity gradient at ten spanwise locations and of the streamwise component U_x of the velocity at seven locations on a line perpendicular to the wall.

2. Conditions for the measurements

Three separate data sets were obtained using different rake positions relative to the wall probes. The rake was placed in the centre at dimensionless distances downstream of $x^+ = 30$, 60 and 90, where the superscript implies the term has been made dimensionless with the friction velocity u^* and the kinematic viscosity ν. During each run the rake was placed at a different distance from the wall. Table 1 presents the dimensionless distances of the fluid probes from the wall along with the downstream distances of the rake from the wall probes. The total dimensionless spanwise length covered by the wall electrodes was 153, which accounts for a dimensionless spanwise spacing of 17 between each adjacent electrode pair.

The rake positions for purposes of data collection were chosen after several test runs were made. If the rake was placed too close to the wall probes, probe interference occurred and the spanwise wall intensities were affected, while the axial wall and fluid probe intensities remained nearly unchanged. Test runs indicated that the dimensionless distance – not the absolute distance – between the rake and the wall probes is critical to probe interference. Reliable measurements were obtained when the rake was placed at $x^+ = 90$ downstream from the wall probes, independent of the y^+ distance of the fluid probes from the wall. It was found that if the rake was placed at $x^+ = 0$ (same position as the wall probes) the first fluid probe had to be at a distance of at least $y^+ = 20$ from the wall to avoid probe interference.

A summary of the experimental conditions is given in table 2, where T_D^+ is the dimensionless time interval, N_D the number of samples, F_S the sampling frequency, E_D the approximate number of events, U_b the bulk velocity, C_b the concentration of iodine in the bulk flow, and D_t the pipe diameter.

3. Use of wall probes to identify events for conditional sampling

3.1. *Types of events sampled*

As indicated in §1, four types of events were identified at $z = 0$: (i) inflows (a large positive value of ds_z/dz); (ii) outflows (a large negative value of ds_z/dz); (iii) large positive spanwise flows (a maximum in $s_z(z)$); (iv) large negative spanwise flows (a minimum in $s_z(z)$). According to the idealized eddy model, inflows and outflows are, on average, coupled in space. Therefore minima or maxima should, on average, be centrally located between an inflow and an outflow.

In addition to focusing on the single events outlined above, it is also of interest to study the behaviour of the flow field when one event succeeds another. In this study we examined situations in which an outflow follows an inflow or in which an inflow follows an outflow.

3.2. *Detection of inflows and outflows*

For inflows and outflows the $s_z(z,t)$ pattern is antisymmetric around the zero-crossing. Thus the sum of the products of its values at equal distances from the zero-crossing is a negative number. In the search for sine-wave-shaped $s_z(z,t)$ patterns in the data set, the spanwise velocity gradients at the wall (at equal distances from the centre of the multiple wall probes) were multiplied and added together. If this summation yielded a positive value then the instant in the data set was rejected as a possible inflow (or outflow) event. The detection process is described by the equation

$$C_1(t) = \frac{\sum_{i=1}^{3} s_z(6-i,t) - s_z(5+i,t)}{\left|\sum_{i=1}^{3} s_z(6-i,t) - s_z(5+i,t)\right|} \sum_{i=1}^{N} s_z(6-i,t)\, s_z(5+i,t), \tag{1}$$

where only negative values of $\Sigma_{i=1}^{N} s_z(6-i,t)\, s_z(5+i,t)$ are considered. In this equation the spanwise velocity gradient $s_z(z,t)$ is expressed as a function of the wall electrode pair q, where q is numbered from 1 to 10. The centre of the multiple wall probes is between probes 5 and 6, and the assumed antisymmetry of the $s_z(z,t)$ pattern requires that inflows and outflows be near this centre location. Inflows and outflows are distinguished by the coefficient of (1); its value is plus unity for outflows and minus unity for inflows. A strong inflow at the centre of the multiple wall probes (i.e. a sine-wave-shaped $s_z(z,t)$ pattern with a large amplitude) generates a large positive value for $C_1(t)$. A violent outflow is assumed to occur near the centre of the multiple wall probes if $C_1(t)$ is a large negative number.

3.3. *Detection of coupled inflows and outflows*

As indicated in figure 1 (*b*), the midpoint of probes 5 and 6 will be centred between a large inflow and outflow if the function describing $s_z(z,t)$ is a cosine wave. The sum of the products of values of $s_z(z,t)$ at equal distances from the midpoint of the probe array results in a positive number. The detection criterion for coupled inflows and outflows can therefore be expressed as

$$C_2(t) = \frac{\sum_{i=1}^{4} s_z(3+i,t)}{\left|\sum_{i=1}^{4} s_z(3+i,t)\right|} \sum_{i=1}^{N} s_z(6-i,t)\, s_z(5+i,t), \tag{2}$$

where only positive values of $\Sigma_{i=1}^{N} s_z(6-i,t)\,s_z(5+i,t)$ are considered. A large positive value of $C_2(t)$ is indicative of a maximum in $s_z(z,t)$ between probes 5 and 6 and therefore a strong counterclockwise eddy. A large negative value of $C_2(t)$ indicates a minimum in $s_z(z,t)$ between 5 and 6 or a clockwise eddy.

3.4. *Dynamic behaviour of inflows and outflows*

If a strong inflow is followed by a strong outflow or if a strong outflow is followed by a strong inflow the variation of the signal at a given location with time will be a sine function. From this consideration it can be seen that a large negative value of the following parameter indicates an outflow–inflow or an inflow–outflow sequence in the $s(z,t)$ pattern around time t:

$$C_3(t) = \sum_{j=1}^{K} \frac{\sum_{i=1}^{3} s_z(6-i,t-j)-s_z(5+i,t-j)}{\left|\sum_{i=1}^{3} s_z(6-i,t-j)-s_z(5+i,t-j)\right|} \sum_{i=1}^{N} s_z(6-i,t-j)\,s_z(5+i,t-j)$$
$$\times \frac{\sum_{i=1}^{3} s_z(6-i,t+j)-s_z(5+i,t+j)}{\left|\sum_{i=1}^{3} s_z(6-i,t+j)-s_z(5+i,t+j)\right|} \sum_{i=1}^{N} s_z(6-i,t+j)\,s_z(5+i,t+j). \tag{3}$$

The criterion $C_3(t)$ involves the sum of the products of $C_1(t)$ taken at different times in the data set:

$$C_3(t) = \sum_{j=1}^{K} C_1(t-j)\,C_1(t+j). \tag{4}$$

The parameter

$$C_4(t) = \frac{\sum_{i=1}^{3} s_z(6-i,t+K)-s_z(6-i,t-K)+s_z(5+i,t-K)-s_z(5+i,t+K)}{\left|\sum_{i=1}^{3} s_z(6-i,t+K)-s_z(6-i,t-K)+s_z(5+i,t-K)-s_z(5+i,t+K)\right|}. \tag{5}$$

was used to indicate the sequence of the detected sine patterns. If $C_4(t)$ is positive an inflow is followed by an outflow. A negative value indicates an outflow following an inflow.

4. Conditional-averaging procedure

All the investigated patterns described in §4 appeared many times in the data set but to different degrees as expressed by solutions to (1)–(5). Crucial to the conditional-averaging procedure is the choice of the threshold level that is applied to the $C_i(t)$ values ($i = 1,2,3,4$) to determine the events in the data set. In this study the conditionally averaged results were found to be insensitive to the applied threshold value, as can be seen in figures 3-4, 3-5 and 3-6 of Hogenes (1979). These figures show the conditionally averaged spanwise velocity gradients at the wall for the condition described by (2). A 20-fold decrease in threshold level resulted in approximately a threefold increase in the number of detected events. Lower threshold levels effected a decrease in the amplitudes of the $s_z(z,t)$ patterns but the specific features of these patterns remained unchanged.

In order to select significant events, one per cent of the data set time was chosen as the event time. As indicated in table 2, 10000 data points were stored for each probe. Thus approximately 100 events were selected for the conditional-averaging

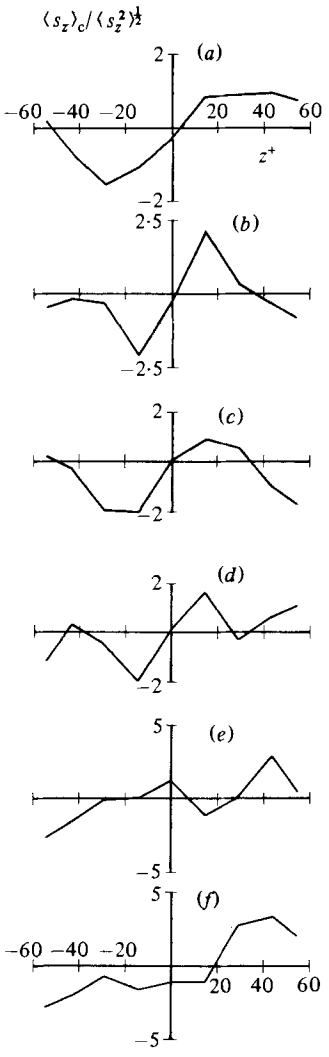

FIGURE 2. Examples of profiles that trigger the detection of a large positive slope at $z = 0$.

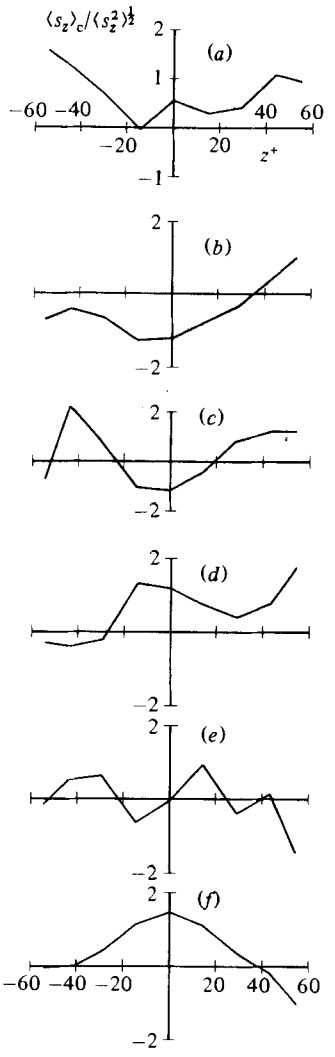

FIGURE 3. Examples of profiles that do not detect a large positive slope at $z = 0$.

procedure. An explanation of why 100 is an acceptable number for the averaging procedure follows.

To detect the coherent eddy structure different intervals of the $s_z(z, t)$ pattern were focused upon as discussed in §3. Equally spaced intervals can be denoted around four characteristic points of the sine-wave-shaped $s_z(z, t)$ pattern: a maximum, a minimum, a positive slope and a zero-crossing, a negative slope and a zero-crossing. Because the $s_z(z, t)$ pattern is random in space the chance α of focusing upon a specified interval of the $s_z(z, t)$ pattern is 25%. The data set has a dimensionless time period of $T_D^+ = 20000$. From figures 3-4, 3-5 and 3-6 of Hogenes (1979) the conditionally averaged duration of the event is found to be approximately $T_E^+ \approx 50$ or about one-half the period between bursts. Thus the number of events E_d in the data set for a given condition can be estimated as

$$E_D = \alpha \frac{T_D^+}{T_E^+} = 0{\cdot}25 \times \frac{20000}{50} = 100.$$

All the instants at which the selected events occurred were labelled $T^+ = 0$. To avoid averaging over the same event more than once, the minimum dimensionless time between each of two consecutive events was longer than $\Delta T^+ = 50$. By counting from these $T^+ = 0$ backwards and forwards in time, points for $T^+ = -26, -24, -22, \ldots, 24, 26$ are denoted. The dimensionless time $T^+ = 2$ between adjacent points corresponds to the frequency at which the analog signals were digitalized. The conditional average of a given event was obtained by taking averages over all the dimensionless time points in the data set of the same numerical value.

For averaging in which large temporal changes were used as the detection criterion (equations (3) and (4)) a value of the parameter K had to be selected. From an examination of conditionally averaged data it was determined that a highly correlated pattern lasted on average for a period ΔT^+ of about 12. Therefore a K of 3 was selected so that the data used in the triggering scheme extended from $T^+ = -6$ to $T^+ = +6$.

Examples of profiles that would trigger the detection of a strong inflow event by (1) are shown in figure 2.† Most of these give a large positive slope of the $s_z(z)$ profile at $z = 0$. However, it is to be noted that the detection scheme is also triggered occasionally on profiles that would not correspond to an inflow at $z = 0$; see e.g. figure 2(*e*).

Examples of profiles that would be rejected by the criterion $C_1(t)$ as a possible inflow or outflow at $z = 0$ are shown in figure 3. Again it is noted that the detection scheme is not perfect. The profile shown in figure 3(*e*) would actually characterize an inflow at $z = 0$.

The reason for the failures of the detection scheme in figure 2(*e*) and 3(*e*) is that a criterion perfectly periodic in the z-direction is being used to examine a non-periodic signal.

5. Description of the experiments

5.1. *Measuring techniques*

The two components of the fluctuating velocity gradient at the wall were measured by electrochemical techniques described in previous papers from this laboratory (Sirkar & Hanratty 1970*b*; Lee *et al.* 1974). The only change is that a different electrochemical system,

$$I_3^- + 2e^- \rightarrow 3I^- \quad \text{(cathode)},$$

$$3I^- \rightarrow I_3 + 2e^- \quad \text{(anode)},$$

was used to get around problems associated with probe contamination.

The fluid velocities were determined by measuring the mass-transfer rate to cylindrical probes placed in the fluid. The probes were operated as cathodes in an electrolysis cell under conditions that they were limited by mass transfer. The electric current flowing to the test electrode is then directly proportional to the mass-transfer rate.

The probes were calibrated by placing them in the centre of the pipeline where the velocity is known. The velocity could be varied by varying the volumetric flow in the pipe. The time-averaged current was measured as a function of the time-averaged velocity and the results fitted with an equation of the form

$$I = BU^n. \tag{6}$$

† The data used in these examples are for a Reynolds number of 13000 and are taken from Lau (1980).

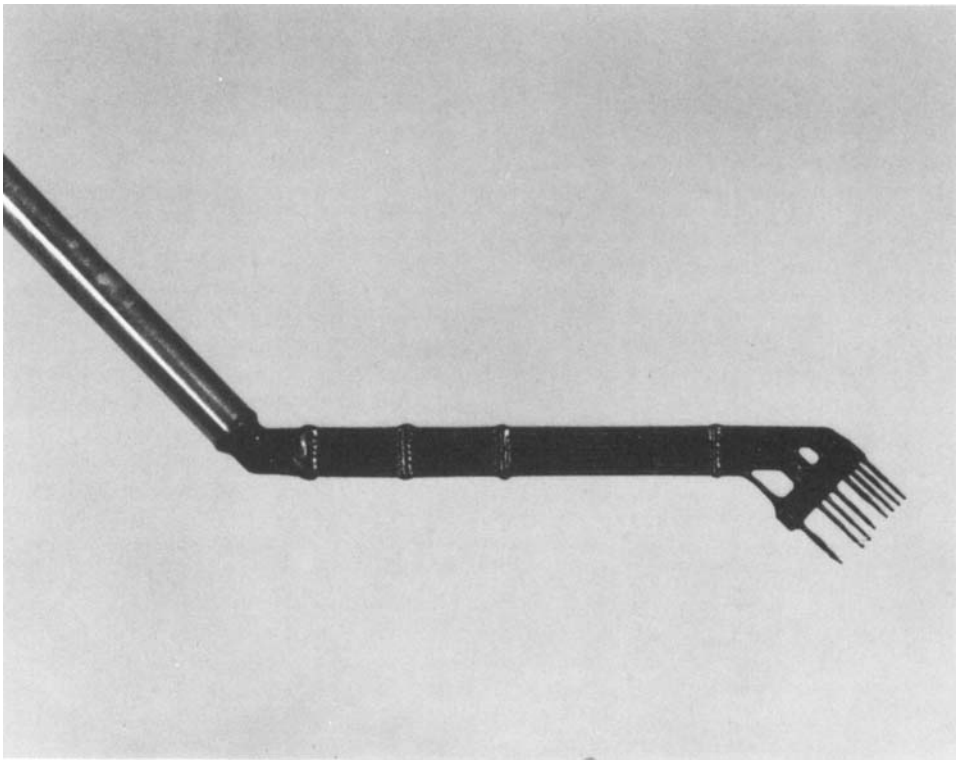

FIGURE 4. Multiple-sensor fluid probe.

The exponent n was found to be equal to 0·39 over a range of probe Reynolds numbers of 1–10.

5.2. *The flow loop*

The experiments were conducted in a vertical, five-level flow system that provides a straight entrance length of 15 m for the 20 cm diameter test section. Details regarding its design are provided in previous publications (Sirkar & Hanratty 1970*a*,*b*; Lee *et al.* 1974).

The wall electrodes are located near the downstream end of the test section. At the top of the test section is a three-dimensional traversing mechanism, operated by three Bodine adjustable-speed torque motors, which permit placement of the fluid probes at any position desired in the test section. The radial and axial displacements of the fluid probe are obtained from linear transducers with a readout accuracy of 0·125 mm. The circumferential readout is obtained with a 40 cm diameter high-accuracy protractor.

5.3. *Multisensor fluid probe*

A multisensor electrochemical fluid probe, custom made by Thermo Systems Inc., was used to measure the velocity in the fluid. Figure 4 shows the fluid probe and its stem, a 6 mm thick shaft that was mounted in the traversing mechanism. Also shown are the long probe needles designed to minimize the blockage effect created by the multiprobe. The bulk flow is parallel to the probe needles, which are kept at a distance of 7 cm from the probe stem by a slender probe body to minimize possible flow

disturbances in the measuring area caused by the stem or the traversing mechanism. The instantaneous axial velocity was measured at seven different radial positions and the instantaneous radial velocity at one position. Probe wire 1 is defined as the extreme right-hand-side wire shown in figure 4. The distance between probe supports 1 and 2 is 1 mm, as is the distance between probe supports 2 and 3, and 3 and 4. Between probe supports 4 and 5 the distance is 2 mm, between 5 and 6 it is 2·25 mm and between 6 and 7 it is 3·75 mm. (Note that 6 and 7 support two cross-wires.) All the wires have diameters of 0·05 mm and sensing lengths of 1·0 mm; thus the length–diameter ratio is 20. High-purity platinum was used as wire material and the gold-plated needle supports were coated with Conothane for electrical insulation. The Reynolds numbers based on the sensor diameter, for maximum and minimum flow in the test section are 34 and 0·6 respectively, and are below the Reynolds number where vortex shedding begins ($R = 44$).

5.4. *Wall electrodes*

The platinum electrodes used to measure the axial and spanwise components of the velocity gradient at the wall were the same as described by Lee *et al.* (1974). A plug containing 40 pairs of electrodes was glued into the wall of the test section. The total spanwise length covered by the 40 pairs was 3·6 cm. The desired dimensionless spanwise length could be realized over a wide range of Reynolds numbers by using the appropriate number of electrodes. The electrodes have sensing widths W of 1·0 mm, sensing lengths L of 0·05 mm and an angle of 15° between them. Details regarding their construction can be found in Hogenes (1979).

6. Results

6.1. *Inflows*

The criterion $C_1(t)$ was used to define $T^+ = 0$ for inflows and outflows and the threshold value of $C_1(t)$ was selected so that approximately 100 events were averaged. Since averaging was done over an interval of $T^+ = -26$ to $T^+ = +26$, the data used in constructing the figures shown in this paper represent approximately $\frac{1}{4}$ of the total time interval studied.

The selection of $N = 5$ in evaluating $C_1(t)$ would mean that all ten wall probes covering a spanwise length of $\Delta z^+ = 153$ are used. Figure 6-5 of Hogenes (1979) shows the conditionally averaged signal for 95 events using $N = 5$. An identifiable inflow pattern starts to emerge at $T^+ = -10$, reaches a maximum amplitude at $T^+ = 0$, and dies out at about $T^+ = 20$. The distance between the minimum and maximum of s_z is $\Delta z^+ = 50$, and there are zero-crossings at $z^+ = \pm 50$. The amplitude at $T^+ = 0$ is about 90 % of the intensity of the spanwise component of the fluctuations in the wall velocity gradient.

The conditionally averaged values of the streamwise component of the fluctuating velocity gradient for this particular sample are shown in figure 6-6 of Hogenes (1979). At $T^+ = -6$ the value of s_x at $z^+ = 0$ starts to increase with time. At $T^+ = 4$ a well-developed pattern with a maximum at $z^+ = 0$ and minima at $z^+ = \pm 50$ is obtained, as suggested by the idealized eddy model in figure 1. This pattern decreases in amplitude after $T^+ = 4$ but appears to persist until $T^+ \approx 24$.

Thus the development of the s_x pattern is found to lag the development of the s_z pattern by a time $\Delta T^+ = 4$. This confirms qualitative observations made by Lee *et al.* (1974). It is also consistent with the measurements of the cross-correlation of s_x and s_z (Lee *et al.* 1974; Blackwelder & Eckelmann 1978, 1979) which show a maximum

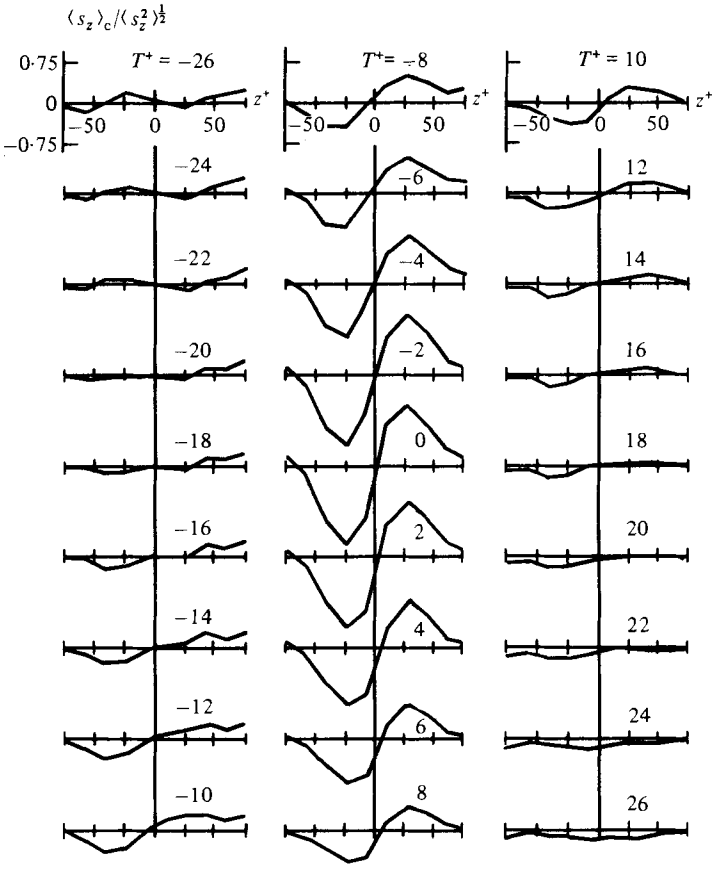

FIGURE 5. Conditionally averaged inflow s_z patterns. Equation (1) with $N = 3$ is applied to s_z gradients; $E_D = 97$.

if s_x is delayed by a small time. As already discussed by Lee *et al.*, this result is anticipated by the idealized eddy model, which suggests that the secondary velocities associated with the flow-oriented eddies are causing the streamwise velocity fluctuations.

The use of $N = 5$ or $\Delta z^+ = 153$ in detecting eddy patterns might not focus accurately enough on happenings at $z^+ = 0$. Therefore it was decided to use $N = 3$ or $\Delta z^+ = 102$ for most of the analysis carried out. Figures 5 and 6 show the s_z patterns and s_x patterns observed for an inflow at $z^+ = 0$ conditionally averaged with $N = 3$ for 97 events. The amplitude of the s_z pattern obtained for $N = 3$ is larger than the amplitude obtained for $N = 5$, having a value of $1{\cdot}5(\overline{s_z^2})^{\frac{1}{2}}$ at $T^+ = 0$. The distance between the maximum and minimum is the same, $\Delta z^+ = 50$. However because the detection scheme only used a Δz^+ of 102 the conditionally averaged pattern is not as well defined for large z^+, and clear-cut zero-crossings at $z^+ = \pm 50$ are not evident. Consistently with the observation of a stronger s_z pattern, the s_z patterns presented in figure 6 for $N = 3$ show larger amplitudes than those found using $N = 5$. The qualitative conclusions about the relation of the evolution of the s_x and s_z patterns is the same for $N = 3$ as for $N = 5$. The s_z pattern begins to emerge at $T^+ = -14$, reaches a maximum at $T^+ = 0$, and dies out at $T^+ = 16$. The s_x lags the s_z pattern by $\Delta T^+ \approx 4$.

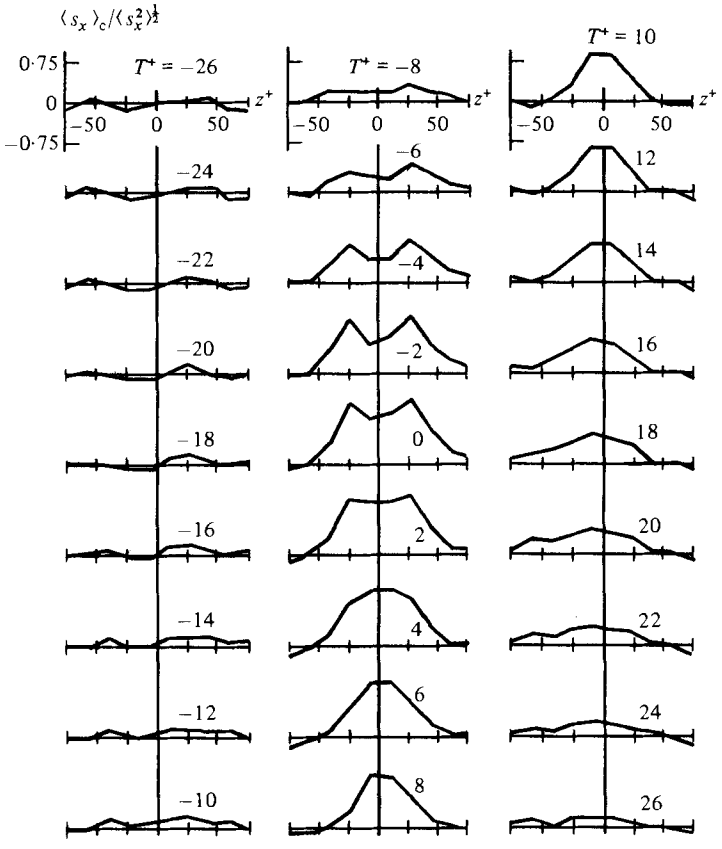

FIGURE 6. Conditionally averaged inflow s_x patterns. Equation (1) with $N = 3$ is applied to s_z gradients; $E_D = 97$.

Measurements of the streamwise velocity components obtained with the rake of probes in the fluid show large momentum excesses close to the wall when inflows are detected from the s_z pattern. Results on the conditionally averaged fluctuations in u_x obtained with the rake located at a distance of $x^+ = 90$ behind the wall probes are shown in figure 7. Measurements with the rake at $x^+ = 30$ and at $x^+ = 60$ are shown in figures 6-11 and 6-12 of Hogenes (1979). The results for $x^+ = 30$ had some unexplained behaviour, which is probably associated with errors in the measurements, so most of the discussion will pertain to results at $x^+ = 60$ and 90.

Measurements at all three x^+ positions showed that the peak in the streamwise velocity fluctuations developed close to the wall. It was not possible to determine the maximum magnitude of this peak because measurements were not made close enough to the wall, but the measurements do show that it occurred at $y^+ < 8$.

Because of spatial variation in the x-direction, the flow patterns downstream were observed to lag those upstream by an amount consistent with the measurements of space–time correlations by Kreplin & Eckelmann (1979) and by Sirkar (1966). From the Kreplin paper we obtain an average dimensionless convection velocity over the viscous wall region of $C_x^+ \approx 15$. This suggests that the patterns in figure 7 lag those at $x^+ = 0$, where the wall probes are located, by $\Delta T^+ \approx 6$. Consequently the pattern in figure 7 at $T^+ = 6$ corresponds to a s_z pattern of maximum amplitude detected at $x^+ = 0$, $T^+ = 0$ and the periods $T^+ = -8$ to 22 and $T^+ = -4$ to 26 correspond to the intervals over which inflow s_z and s_x patterns would be observed at $x^+ = 90$. The

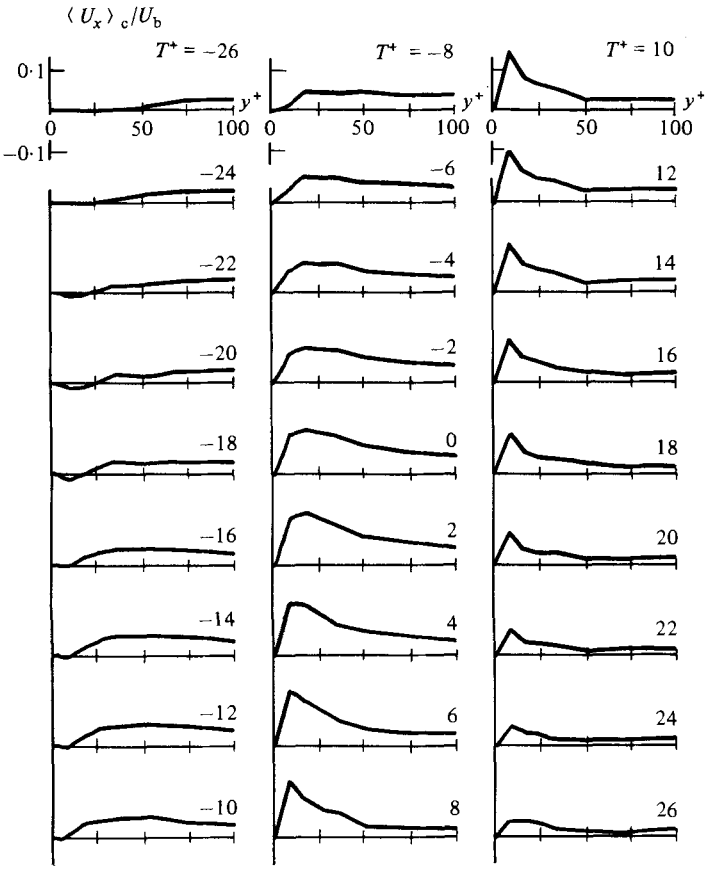

FIGURE 7. Conditionally averaged inflow u_x patterns. Equation (1) with $N = 3$ is applied to s_z gradients; $E_D = 100$; fluid probes at $x^+ = 90$.

peak in the streamwise velocity fluctuations that appears close to a wall from $T^+ \approx -4$ to 26 can therefore be associated with the inward movement of high-momentum fluid, which creates a proportionately larger velocity increase near the wall than farther out, $y^+ > 30$.

The interpretation of other aspects of the profiles in figure 7 requires a recognition that it takes a finite time for disturbances in the outer flow to propagate to the wall (Hatziavramidis & Hanratty 1979; Kreplin & Eckelmann 1979). From the measurements of Kreplin & Eckelmann an inflow s_z pattern, which we estimated earlier to be initiated at $x^+ = 90$ at $T^+ = -8$, would have been first observed at $y^+ = 50$, 25 and 10 at times $T^+ \approx -32$, -24 and -16. The appearance of high-momentum fluid over the period $T^+ = -26$ to -4 can therefore be associated with the propagation of disturbances from the outer flow to the wall.

From the measurements of the s_x and s_z patterns we obtained a period for an observable disturbance of $T^+ \approx 30$. If this same estimate holds at the outer edge of the viscous wall region it would mean that at $y^+ = 50$ the inflow disturbance in u_z that originated at $T^+ \approx -32$ would subside at $T^+ \approx -2$. It is observed in figure 7 that u_x at $y^+ = 50$ starts to decrease with increasing time at $T^+ = 2$. Thus the subsidence of u_x at $y^+ = 50$ corresponds closely to the subsidence of the inflow pattern at that location.

The results shown in figure 8 were obtained by adding the conditionally averaged

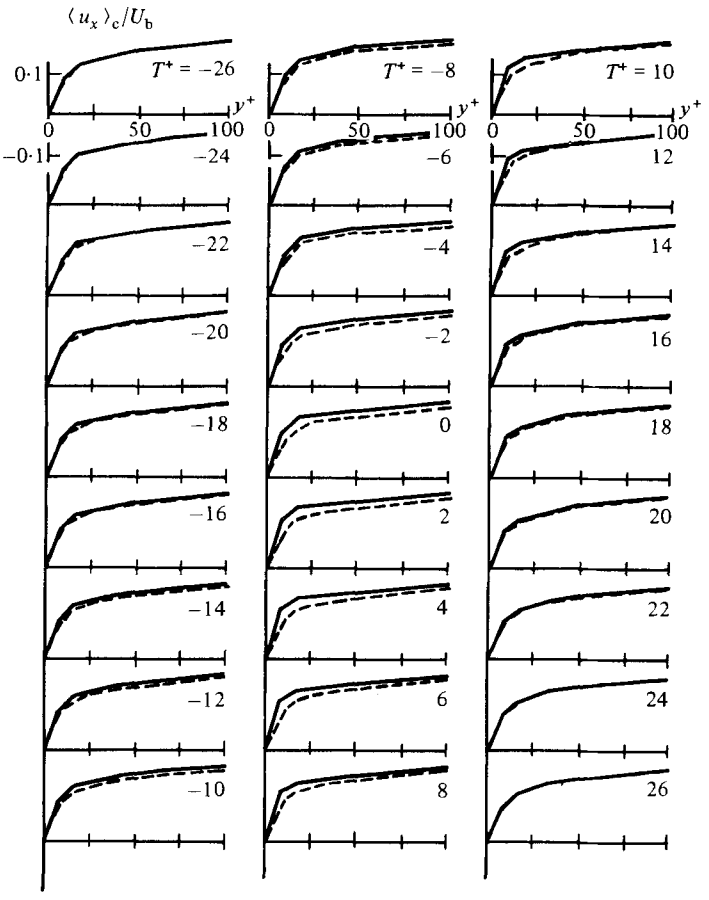

FIGURE 8. Conditionally averaged inflow U_x patterns. Equation (1) with $N = 3$ is applied to s_z gradients; $E_D = 97$; fluid probe at $x^+ = 60$; ---, mean-velocity profile; ——, conditionally averaged pattern.

fluctuating velocities shown in figure 6-12 of Hogenes (1979) to the local mean velocities. The solid lines represent the conditionally averaged velocity profiles and the dashed lines represent the mean profiles. These clearly show a flattening of the velocity profile, particularly during the period when the fluctuations showed a large peak near the wall. No evidence of inflectional profiles was found.

6.2. *Outflows*

Figure 9 shows s_z profiles conditionally averaged for an outflow using $C_1(t)$ with $N = 3$. A total of 98 events were selected. A sinusoidal profile starts to develop at $T^+ = -16$, has a maximum amplitude at $T^+ = 0$, and disappears at about $T^+ = 14$. The length and the amplitude of the pattern is approximately the same as had been found for an inflow. This would indicate that inflows and outflows are of the same magnitude, as is suggested by the idealized eddy model.

The conditionally averaged measurements of s_x for an outflow are shown in figure 10. A faint inflow pattern is indicated for $T^+ = -26$ to -10. A s_x profile, characteristic of an outflow, starts to develop; at $T^+ = 6$ a strong outflow pattern with a distance between zero-crossings of $\Delta z^+ = 50$ is established. After $T^+ = 6$ the amplitude decreases until at about $T^+ = 22$ it disappears. A time interval $\Delta T^+ = 6$ occurs

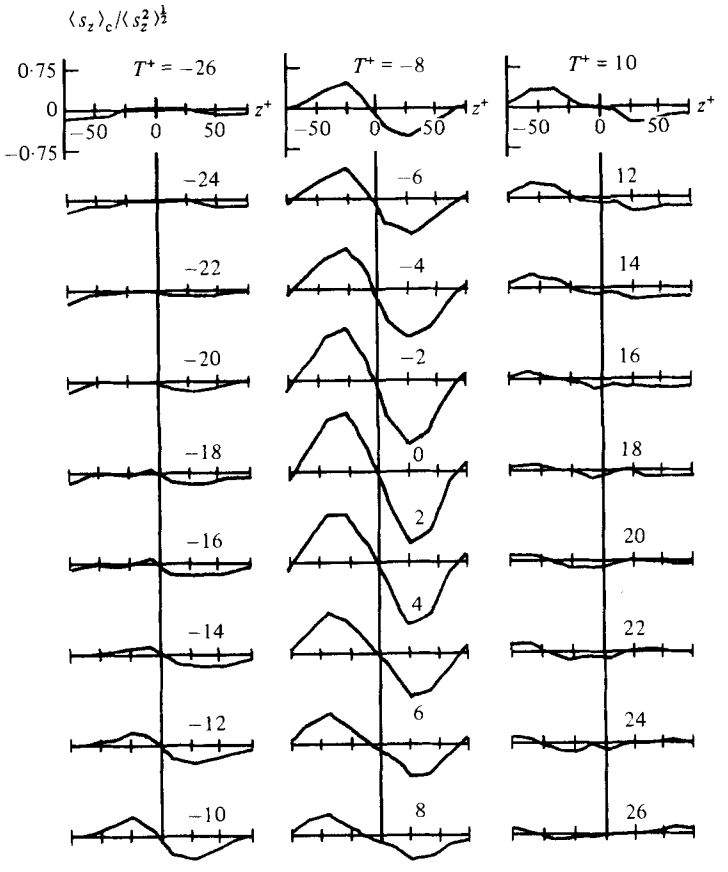

FIGURE 9. Conditionally averaged outflow s_z patterns. Equation (1) with $N = 3$ is applied to s_z gradients; $E_D = 98$.

between the appearance of the maximum-amplitude s_z pattern and the maximum-amplitude s_x pattern.

Measurements of the streamwise velocity fluctuations conditionally averaged for an outflow are presented in figure 11 for the rake located at $x^+ = 60$. Again, assuming that the pattern is convected downstream with a velocity $C_x^+ = 15$, we argue that the profiles in figure 11 are representative of what would be measured at $x^+ = 0$ for time $T^+ = \Delta T^+$ where $\Delta T^+ = 4$. Consequently $T^+ = 4$ in figure 11 corresponds to a s_z pattern of maximum amplitude detected at $x^+ = 0$, $T^+ = 0$, and the periods $T^+ = -12$ to 18 and $T^+ = -4$ and 26 correspond to the duration of the s_z and s_x patterns at $x^+ = 60$.

The profile of streamwise velocity fluctuations develops a minimum at $y^+ \approx 19$ at $T^+ = -6$. The minimum moves into the region $y^+ < 11$ at $T^+ = 10$, and dies out at $T^+ = 24$. This minimum has a duration roughly equal to that of the outflow s_z pattern, and lags it by $\Delta T^+ = 6$. It therefore appears that the development of this minimum is associated with the outward flow of low-momentum fluid from the wall.

Using the arguments presented in the discussion of inflows we estimate that a disturbance in the spanwise velocity components giving rise to the observed outflow at the wall was initiated outside the viscous wall region and appears at $y^+ = 50$, 19 and 11 at times that would correspond to $T^+ = -36$, -26 and -20 in figure 11.

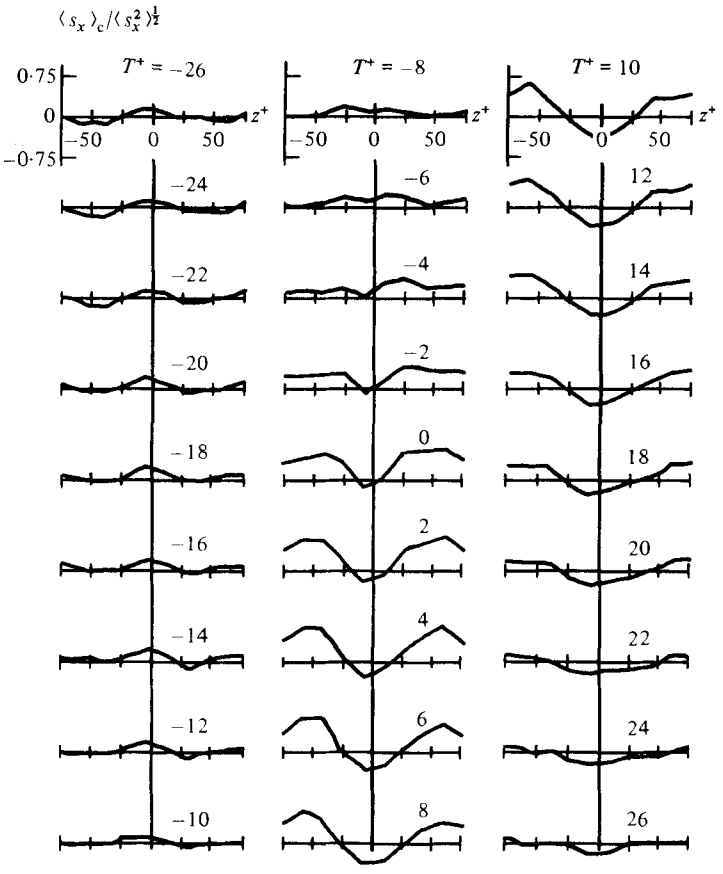

FIGURE 10. Conditionally averaged outflow s_x patterns. Equation (1) with $N = 3$ is applied to s_z gradients; $E_D = 98$.

However, unlike the inflows, there is no indication of the movement of a wave of negative momentum toward the wall. In fact, for outflows significant velocity fluctuations do not appear in the field over the time interval $T^+ = -26$ to -12.

Again, if it is estimated that the lifetime of the disturbance is $\Delta T^+ = 30$, then the outflow would disappear at $y^+ = 19$, $T^+ = 4$ and at $y^+ = 11$, $T^+ = 10$. It is noted in figure 11 that the magnitude of the negative deviations in u_x starts to decrease at $y^+ = 19$, $T^+ = 8$ and at $y^+ = 11$, $T^+ = 12$. Thus the beginning of the decay of the fluctuation at a given value of y could be associated with the termination of the outflow disturbance at that location.

Figure 12 results from adding the conditionally averaged fluctuating velocities in figure 11 to the local mean velocities. The solid line represents the conditionally averaged velocity profile and the dashed line represents the mean-velocity profile. From $T^+ = -26$ to -8 the conditionally averaged velocity is nearly the same as the local mean velocity. Inflections in the conditionally averaged profile at $y^+ = 20$ and at $y^+ = 30$ are indicated from $T^+ = 0$ to 8. This would correspond to the maximum interaction between the viscous wall region and the outer flow (bursting?), and to the period when the s_z profiles have well-developed outflow patterns (see figure 9 from $T^+ = -4$ to 4).

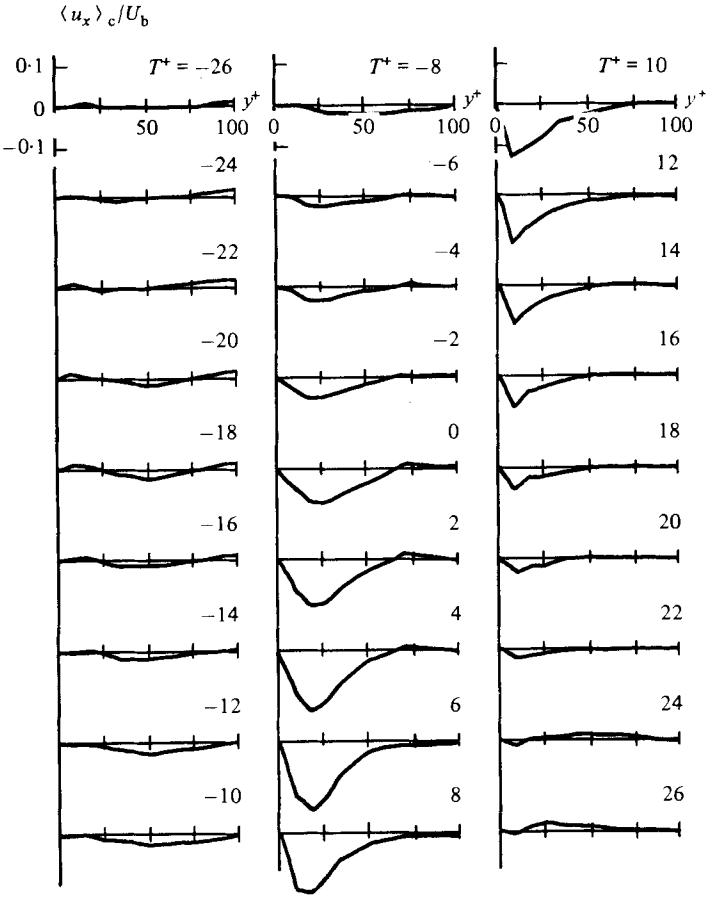

FIGURE 11. Conditionally averaged outflow u_x patterns. Equation (1) with $N = 3$ is applied to s_z gradients; $E_D = 98$; fluid probes at $x^+ = 60$.

6.3. *Coupled inflows and outflows*

By applying condition $C_2(t)$ with $N = 4$ to spanwise velocity gradients at the wall the coupling of inflows and outflows could be investigated. Figure 13 shows the results from conditionally averaging 100 samples. A pattern with a spacing between maxima of $\Delta z^+ \approx 100$ begins to evolve at $T^+ = -16$, reaches a maximum amplitude at $T^+ = 0$, and disappears at $T^+ = 10$.

The conditionally averaged s_x measurements in figure 14 show sine-wave profiles with a maximum, suggesting an inflow of high-momentum fluid, at $z^+ = 25$ and a minimum, suggesting the outflow of low-momentum fluid, at $z^+ = -25$. This pattern starts to develop at $T^+ = -6$ and disappears at $T^+ = 24$.

Results of the same type were obtained if the conditional-averaging technique focused on a maximum in s_z at $z^+ = 0$. However, in this case an outflow of low-momentum fluid occurs at $z^+ = 25$ and an inflow of high-momentum fluid occurs at $z^+ = -25$.

Measurements of conditionally averaged velocity profiles in the fluid using condition $C_2(t)$ were found to be not very different from the mean profiles. This suggests that large changes of the velocity profile occur primarily at spanwise locations where large inflows and outflows are indicated by the measurements of s_z.

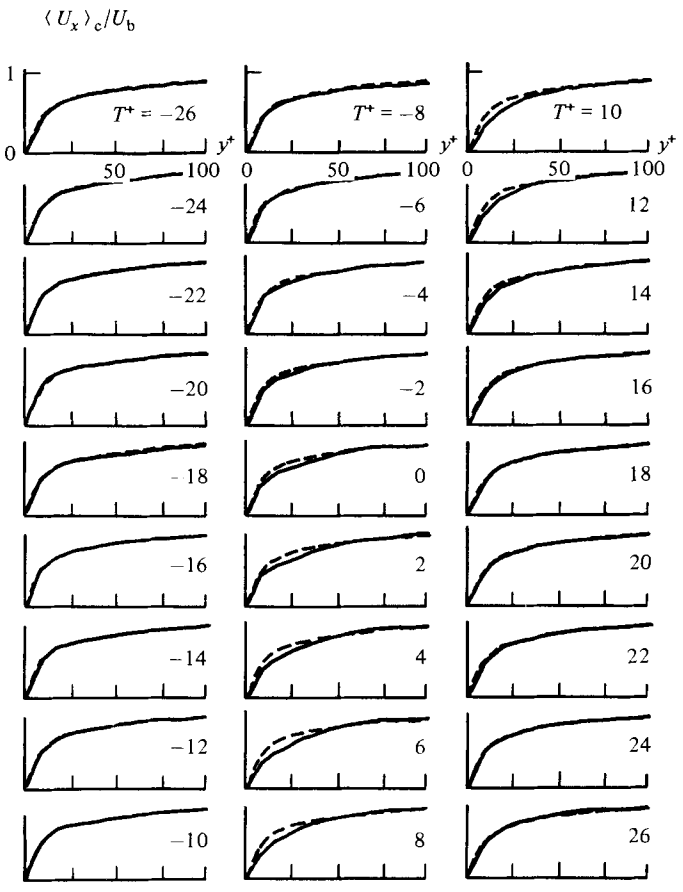

FIGURE 12. Conditionally averaged outflow U_x patterns. Equation (1) with $N = 3$ is applied to s_z gradients; $E_D = 98$; fluid probes at $x^+ = 60$; ---, mean-velocity profile; ——, conditionally averaged pattern.

6.4. *Dynamic behaviour of inflows and outflows*

The detection of profiles with shear layers during outflows prompted the investigation of situations in which an inflow immediately followed, or was followed by, an outflow in order to see if the effect could be made more dramatic. To do this $C_3(t)$ was used with $N = 3$ and $K = 4$. Seventy outflow–inflow sequences and 66 inflow–outflow sequences were selected for conditional averaging.

Results are given in figures 15–18 for an outflow–inflow sequence and in figures 6-29–6-33 of Hogenes (1979) for an inflow–outflow sequence. The selection of about 70% of the samples used to detect a pure outflow or a pure inflow implies that we were assuming that there is a $\frac{2}{3}$ chance that an outflow is followed by an inflow. As seen in figure 15, the s_z profiles detected are of lower amplitude than those shown in figures 5 and 9. This suggests that a smaller sample should have been selected and that the probability that an inflow follows an outflow is closer to $\frac{1}{3}$ than to $\frac{2}{3}$.

Our choice of a sample that is too large implies that it included a number of events which were not desired. This is evident in the s_x profiles, which are not as well developed as those shown in figures 6 and 10. However, despite these shortcomings in the sample size, the results are of interest because they show in a dramatic way

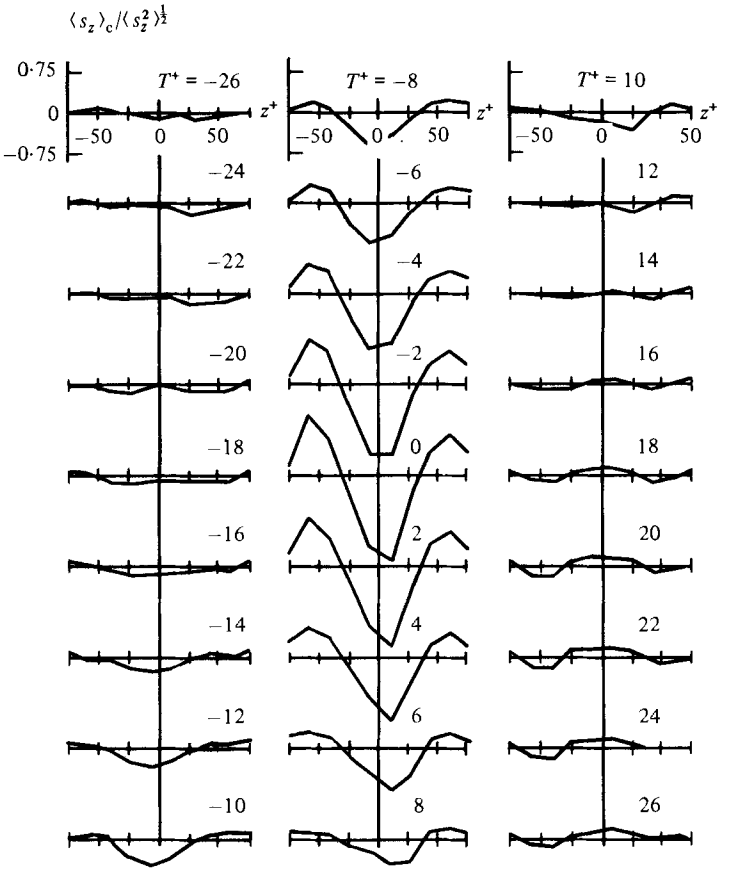

FIGURE 13. Conditionally averaged inflow–outflow s_z patterns. Equation (2) is applied to s_z gradients; $E_D = 100$.

how the streamwise velocity fluctuations are controlled by the secondary flow, detected through measurements of s_z.

Figure 15 shows the emergence of an outflow s_z pattern at $T^+ = -20$. This pattern grows in strength until at $T^+ = -8$ the conditionally averaged s_z measurements show an amplitude equal to $0{\cdot}75(\overline{s_z^2})^{\frac{1}{2}}$. With further increase in time the amplitude of the pattern decreases. From $T^+ = -2$ to 2 the outflow pattern changes to an inflow pattern. The inflow pattern increases in amplitude until $T^+ = 8$, and after that time decays until at $T^+ = 20$ it is barely perceptible.

The outflow pattern starts to develop in the s_x measurements at $T^+ = -16$. The trough that appears at $z^+ = 0$ reaches its maximum value at $T^+ = 0$, when the s_z pattern has subsided. A well-developed outflow s_x pattern persists until $T^+ = 8$, even though an inflow pattern at the wall has been initiated. A rather poorly defined inflow s_x pattern starts to emerge at $T^+ = 10$, and is still in evidence at $T^+ = 26$ after the inflow s_z pattern has subsided.

The measurements of the fluctuations in u_x in figure 17 show a pronounced minimum close to the wall, which can be associated with an outflow pattern in the viscous wall region at $z^+ = 0$. It is of interest to note how this minimum is annihilated with the change of the pattern. A wave of positive momentum is observed to move

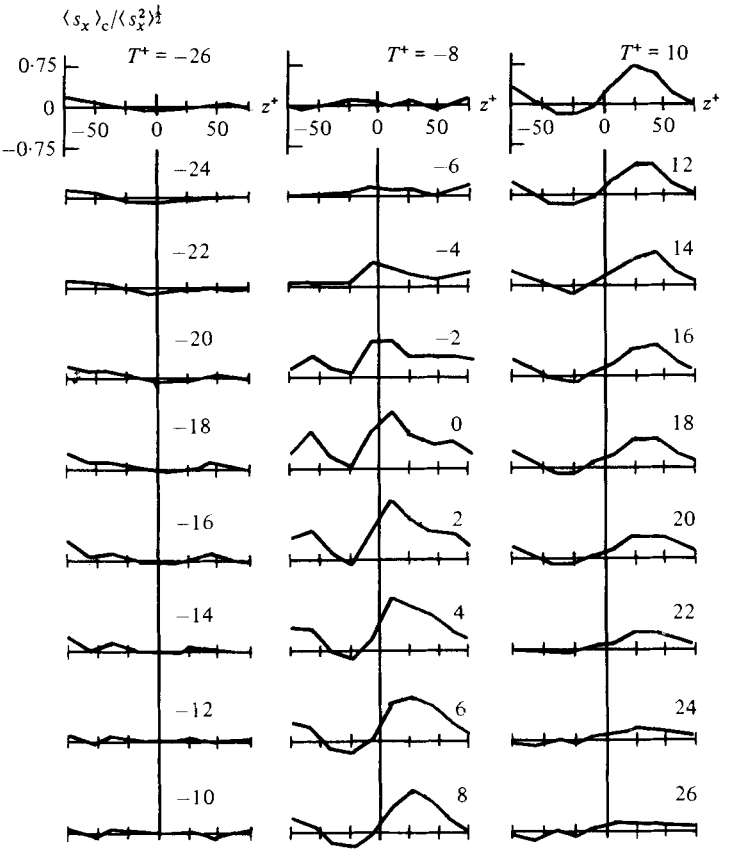

FIGURE 14. Conditionally averaged inflow–outflow s_x patterns. Equation (2) is applied to s_z gradients; $E_D = 100$.

from $y^+ = 40$, $T^+ = 2$ to the wall at $T^+ = 10$. This is interpreted as being associated with an inflow disturbance moving from the outer flow to the wall.

The profiles in figure 18, obtained by adding the fluctuations in u_x to averaged velocity measurements, show the change of the conditionally averaged measurements from an inflectional profile to one that is blunter than the time-averaged measurements.

Results on inflow–outflow sequences discussed in Hogenes (1979) are similar to those obtained for outflow–inflow sequences.

7. Significance of results

This paper proposes that multipoint measurements are a sounder means to detect spatial aspects of eddy structures than are single-probe measurements, which give a time signature of the velocity at a fixed location in the field. It demonstrates the application of such an approach to study the flow-oriented eddies that have been detected in the viscous wall region of a turbulent flow. The particular algorithms used to analyse the multipoint measurements accomplished our goals but they are not considered final. In fact we have achieved considerable improvements in these detection schemes in more recent studies.

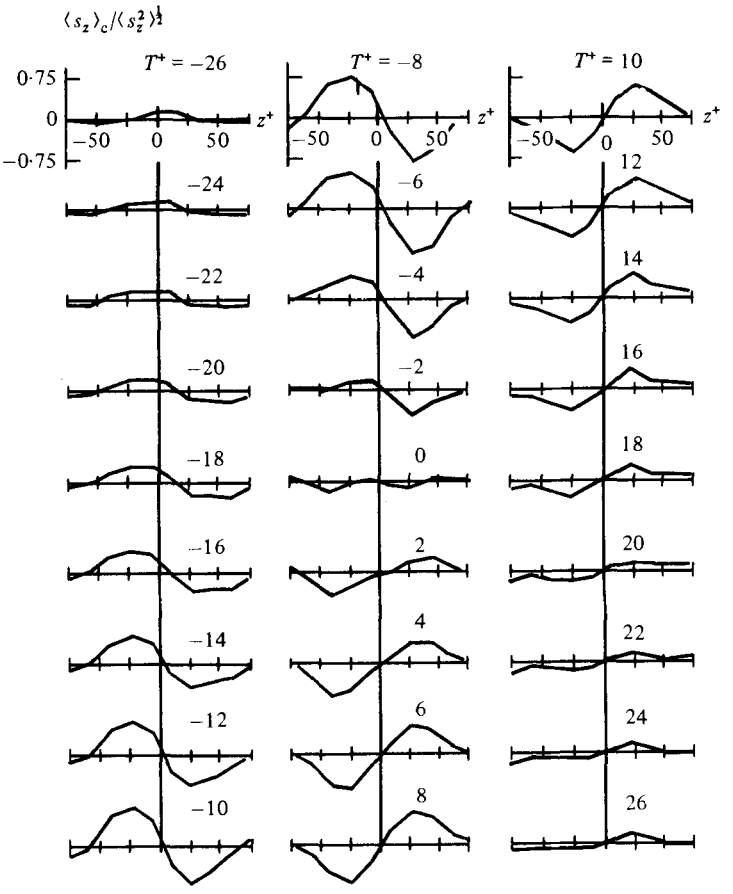

FIGURE 15. Conditionally averaged transitional outflow–inflow s_z patterns. Equation (3) is applied to s_z gradients; $E_D = 70$.

Most previous work on conditional averaging in the viscous wall region has focused on the detection of the bursting phenomenon. We have taken a different approach in that we have used an idealized eddy model developed by Sirkar & Hanratty to identify four aspects of the wall eddies from measurements of $s_z(z, t)$: (i) large inflows at $z^+ = 0$; (ii) large outflows at $z^+ = 0$; (iii) large positive spanwise flows at $z^+ = 0$ (counterclockwise eddies); and (iv) large negative spanwise flows at $z^+ = 0$ (clockwise eddies). Inflectional profiles of the streamwise velocity are observed for a period of $\Delta T^+ \approx 8$ when the s_z profiles give outflow patterns of maximum amplitude. This would indicate periods of large outflows and of strong interaction with the outer flow that could correspond to the bursting phenomenon defined in visual experiments. However, the conditional-averaging scheme used by us yields a duration time of $\Delta T^+ \approx 30$ for an observable pattern. If we assume an interval of $\Delta T^+ \approx 10$ between patterns we obtain an estimate of an average period between the development of large-amplitude s_z profiles of $\Delta T^+ \approx 40$. Since each of these profiles would indicate a strong outflow somewhere over the interval $-50 < z^+ < 50$, we obtain an estimate of the interval between bursts of $\Delta T^+ = 40$. This appears to be too low by a factor of 2–3. This could mean that our detection schemes underestimate the duration of events, since we are using fixed probes to capture eddies that have a certain amount

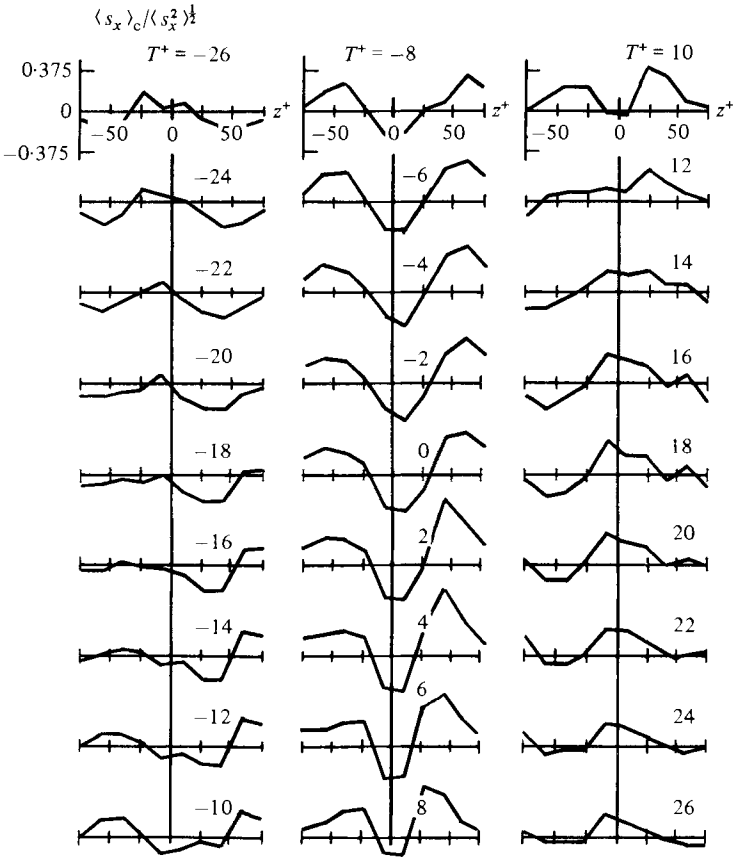

FIGURE 16. Conditionally averaged transitional outflow–inflow s_x patterns. Equation (3) is applied to s_z gradients; $E_D = 70$.

of 'jitter'. However, it could also mean that every strong outflow might not end up in a visually detected burst.

We find that the outflow s_z patterns grow and decay symmetrically in time around $T^+ = 0$. This indicates that large outflows are not jetlike motions that suddenly appear. On the contrary, they have a temporal behaviour similar to what would be found for a cosine function with a period of $\Delta T^+ = 2 \times 40 = 80$, which is of the same magnitude as the period of the most-energetic fluctuations of the velocity close to the wall. The jetlike eruptions discussed in the literature would seem to require the sudden development of small-scale variations of the flow in the streamwise direction. This could come about by an interaction of negative-momentum flow that has been moved out from the wall with the outer flow.

In this paper we have focused on the role of the secondary flows at the wall in creating large streamwise velocity fluctuations and in generating the low-momentum fluid that has been observed to emerge from the wall. Consequently we have given particular attention to the inflow and outflow modes, since the streamwise velocity profiles are observed, on average, to be similar to the time-averaged velocity profile during periods of strong spanwise flows at $z^+ = 0$. In another paper (Nikolaides *et al.* 1982), in which we examine the relation of the wall structures to spanwise velocity fluctuations in the region $y^+ = 20$–40, we find the s_z patterns, which indicate

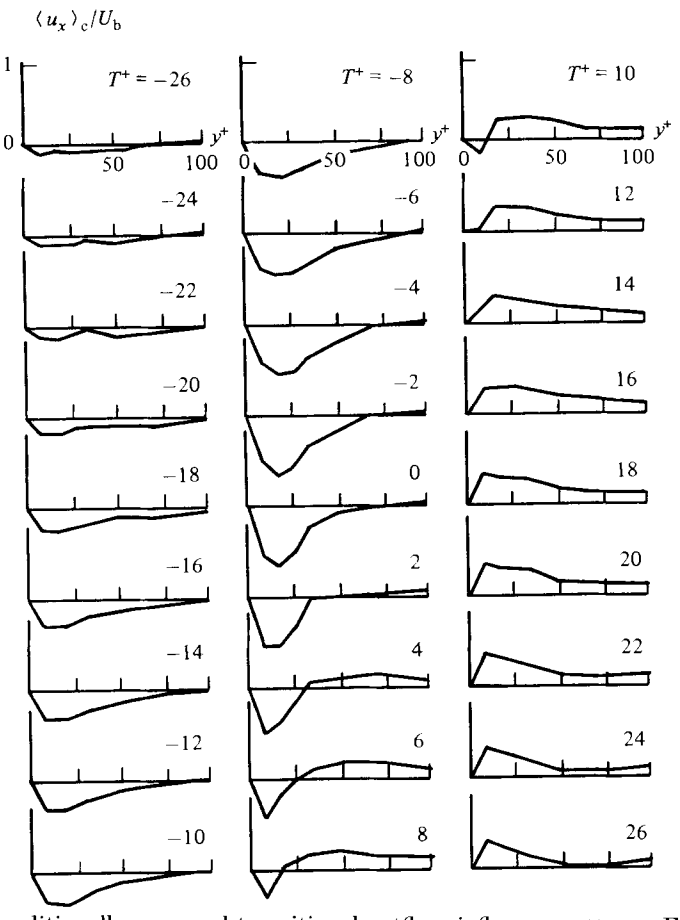

FIGURE 17. Conditionally averaged transitional outflow–inflow u_x patterns. Equation (3) is applied to s_z gradients; $E_D = 78$; fluid probes at $x^+ = 90$.

strong spanwise flows at $z^+ = 0$ to be particularly useful as a criterion for conditionally averaging measurements of the spanwise component of the velocity fluctuations.

The results presented in this paper are consistent with the idealized picture of the wall eddies suggested by Sirkar & Hanratty and further developed by Fortuna and by Hatziavrimidis. The inflows and outflows at the wall are of equal magnitude, are, on average, coupled in the z-direction, and have a spacing of $z^+ = 50$. The development of strong streamwise velocity fluctuations is found to lag the development of strong secondary flows, as evidenced by the s_z profiles. This supports the notion that the disturbance in the flow associated with these s_z profiles is causing large fluctuations in the streamwise velocity.

These disturbances are pictured by us as originating in the region outside the viscous wall region and as associated with turbulent spanwise deviations in the velocity. As shown by Hatziavramidis & Hanratty (1979) in their periodic-eddy model, the flow at the wall does not respond immediately to changes in the spanwise flow at $y^+ = 30$–50. This lag in the motion at the wall can be described by assuming that the disturbances in s_z propagate to the wall. The calculations of Hatziavramidis indicate a time of $T^+ \approx 15$ for the disturbances to travel from $y^+ = 30$ to the wall. A more-accurate value of $T^+ \approx 22$ is obtained from the

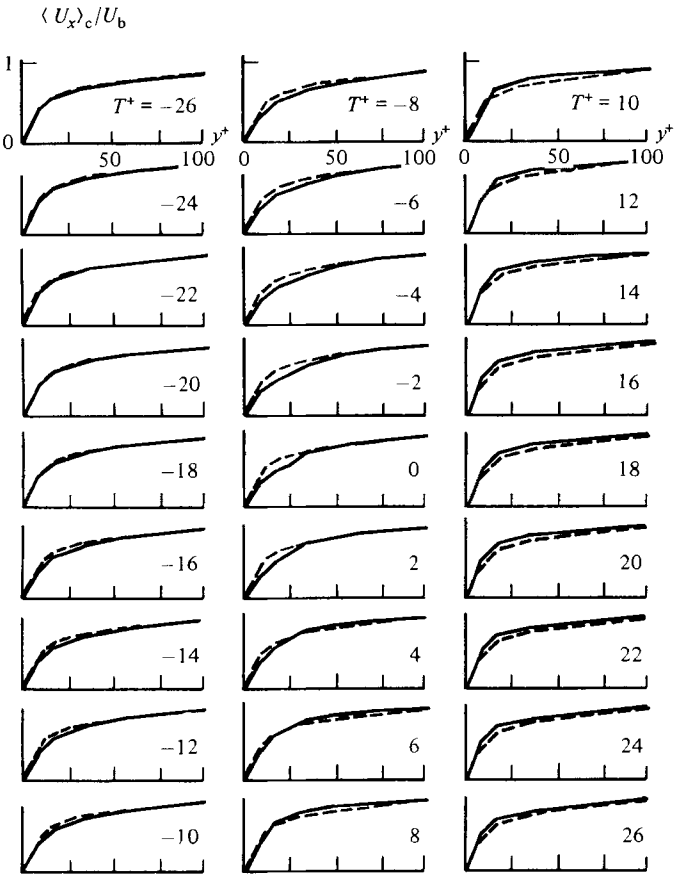

FIGURE 18. Conditionally averaged transitional outflow–inflow U_x patterns. Equation (3) is applied to s_z gradients; $E_D = 78$; fluid probes at $x^+ = 90$; ---, mean-velocity profile; ——, conditionally averaged pattern.

correlation measurements of Kreplin & Eckelmann. It is of interest that these periods are about half of the duration time of a disturbance observed in this research. This means that, by the time the disturbance has reached its maximum activity at the wall, it has subsided at $y^+ = 30$, and a new flow mode is being propagated from $y^+ = 30$ to the wall. The incorporation of this notion of disturbances propagating to the wall with the eddy model of Sirkar & Hanratty provides a theoretical picture that is consistent with our measurements of conditionally averaged streamwise velocity fluctuations. We examined briefly the question of whether one particular disturbance mode at $y^+ = 30$ facilitates its succession by another particular mode by conditionally averaging for an outflow s_z pattern followed by an inflow s_z and for an inflow followed by an outflow. We have tentatively concluded that there is an approximately $\frac{1}{3}$ chance that an inflow will follow an outflow. This means that an inflow pattern is not likely to be followed by another inflow pattern. However, the experiments on which this conclusion is based are of limited extent and the matter needs to be explored further.

The model used by Hatziavramidis assumes homogeneity in the x-direction. To account for changes of the eddy pattern in the flow direction, we have simply used the notion of a convection velocity, whereby we assume that the type of changes which

Hatziavramidis calculates to occur over a time interval ΔT^+ will also be observed over a space interval of $\Delta x^+ = C_x^+ \Delta T^+$. This approach ignores small-scale changes in the flow directions.

The type of results presented in this paper supports the notion that flow-oriented wall eddies, approximately homogeneous in the flow direction, are playing an important role in the momentum-exchange process between the wall and the fluid and in the transfer of energy from the mean flow to the fluctuating flow. However, it is not clear that they are completely controlling. The research presented here has ignored the influence of all small-scale turbulence in the flow direction and the influence of eddies with lengths much less than $\lambda^+ = 100$ in the z-direction. Yet it is quite possible that such small-scale turbulence is making important contributions to the Reynolds stress in the viscous wall region. This appears to be an issue that deserves more attention. Current research in which we are trying to relate mass-transfer rates to eddy structure (Campbell 1981) has shown that mass-transfer rates to a solid wall will be underestimated by a large amount if the influence of small-scale turbulence is not taken into account.

This work is supported by the Office of Naval Research under Grant NR 062-558. We also gratefully acknowledge the work done by Dr D. P. Zilker in designing and assembling the probe mechanism.

REFERENCES

BAKEWELL, H. P. & LUMLEY, J. L. 1967 *Phys. Fluids* **10**, 1880.

BLACKWELDER, R. F. & ECKELMANN, H. 1978 In *Structure and Mechanisms of Turbulence I* (ed. H. Fiedler), p. 190. Lecture Notes in Physics, vol. 75. Springer.

BLACKWELDER, R. F. & ECKELMANN, H. 1979 *J. Fluid. Mech.* **94**, 577.

BLACKWELDER, R. F. & KAPLAN, R. E. 1976 *J. Fluid Mech.* **76**, 89.

CAMPBELL, J. A. 1981 Ph.D. thesis, University of Illinois, Urbana.

COLES, D. 1978 In *Proc. Workshop in Coherent Structure of Turbulent Boundary Layers*, Lehigh University, Bethlehem, Pennsylvania (ed. C. R. Smith & D. E. Abbot), p. 462.

CORRSIN, S. 1956 In *Proc. Symp. on Naval Hydrodynamics*, p. 373.

FORTUNA, G. 1971 Ph.D. thesis, University of Illinois, Urbana.

GRANT, H. L. 1958 *J. Fluid Mech.* **4**, 149.

HANRATTY, T. J., CHORN, L. G. & HATZIAVRAMIDIS, D. T. 1977 *Phys. Fluids Suppl.* **20**, S112.

HATZIAVRAMIDIS, D. T. & HANRATTY, T. J. 1979 *J. Fluid Mech.* **95**, 655.

HOGENES, J. H. A. 1979 Ph.D. thesis, University of Illinois, Urbana.

KIM, H. T., KLINE, S. J. & REYNOLDS, W. C. 1971 *J. Fluid Mech.* **50**, 133.

KLINE, S. J., REYNOLDS, W. C., SCHRAUB, F. A. & RUNSTADLER, P. W. 1967 *J. Fluid Mech.* **30**, 741.

KLINE, S. J. & RUNSTADLER, P. W. 1959 *Trans. A.S.M.E.* E: *J. Appl. Mech.* **26**, 166.

KREPLIN, H. P. & ECKELMANN, H. 1979 *J. Fluid Mech.* **95**, 305.

LAU, K. K. 1980 Ph.D. thesis.

LEE, M. K., ECKELMAN, L. D. & HANRATTY, T. J. 1974 *J. Fluid Mech.* **66**, 17.

MCCONAGHY, G. A. & HANRATTY, T. J. 1977 *A.I.Ch.E. J.* **23**, 493.

NIKOLAIDES, C., LAU, K. K. & HANRATTY, T. J. 1982 Submitted for publication.

OFFEN, G. R. & KLINE, S. J. 1974 *J. Fluid Mech.* **62**, 223.

REISS, L. P. & HANRATTY, T. J. 1962 *A.I.Ch.E. J.* **8**, 245.

REISS, L. P. & HANRATTY, T. J. 1963 *A.I.Ch.E. J.* **9**, 154.

SIRKAR, K. K. 1966 M.S. thesis, University of Illinois, Urbana.

SIRKAR, K. K. & HANRATTY, T. J. 1970*a* *J. Fluid Mech.* **44**, 589.

Sirkar, K. K. & Hanratty, T. J. 1970*b* *J. Fluid Mech.* **44**, 605.

Townsend, A. A. 1958 In *Proc. IUTAM Symp. om Grenzschichtforschung, Freiburg* (ed. H. Görtler), p. 1. Springer.

Willmarth, W. W. 1975 *Adv. Mech.* **15**, 159.

Willmarth, W. W. & Lu, S. S. 1971 *J. Fluid Mech.* **55**, 481.

Willmarth, W. W. & Tu, B. J. 1967 *Phys. Fluids Suppl.* **10**, S134.